Available at
www.ElsevierComputerScience.com
POWERED BY SCIENCE DIRECT®

Signal Processing 86 (2006) 2139–2152

SIGNAL PROCESSING

www.elsevier.com/locate/sigpro

Cyclic-mean based synchronization and efficient demodulation for UWB ad hoc access: Generalizations and comparisons ☆

Xiliang Luo, Georgios B. Giannakis*

Department of Electrical and Computer Engineering, University of Minnesota, 200 Union Street, Minneapolis, MN 55455, USA

Received 3 January 2005; accepted 15 June 2005
Available online 21 February 2006

Abstract

Synchronization is a performance-critical factor in all communication systems, but becomes particularly challenging in ultra-wideband (UWB) radios due to the ultra-short length of the transmitted pulses. Presence of severe inter-symbol interference (ISI) and multi-user interference (MUI) render the synchronization task even more difficult. The present paper deals with a blind synchronization and demodulation scheme which relies on intermittent transmission of nonzero mean symbols. This transmission pattern enables MUI- and ISI-resilient timing acquisition via energy detection and low-complexity demodulation by correlating the received waveform with a synchronized aggregate template (SAT). The resultant SAT receiver offers distinct advantages over the traditional RAKE and has remarkably low-complexity. Its blind operation nicely fits the requirements of multi-user ad hoc access and its ability to handle ISI is particularly attractive for UWB communications. Analytical performance evaluation of the novel timing estimator and the SAT demodulator is provided along with comparisons with the RAKE receiver for a single user link without ISI. Simulations confirm the analytical results and corroborate the high potential SAT-based UWB modems have for deployment.

Keywords: Synchronization; Timing offset estimation; Blind receivers; Ultra-wideband (UWB); Ad hoc multiple access; Wireless sensor networks

1. Introduction

Timing synchronization is a task particularly challenging coherent reception of ultra-wideband (UWB) signals, because the information conveying pulses are ultra-short (in the order of a nanosecond in impulse radios) [1]. A number of algorithms have been developed recently to address this challenge. Certain training-based UWB synchronizers assume absence of inter-frame interference (IFI) [2] or inter-symbol interference (ISI) [3]; while others require formidable processing complexity [4]. The blind timing algorithm in [5] can cope with IFI, but this

☆This work was supported by the NSF-ITR Grant No. EIA-0324864, and through collaborative participation in the Communications and Networks Consortium sponsored by the U.S. Army Research Laboratory under the Collaborative Technology Alliance Program, Cooperative Agreement DAAD19-01-2-0011. The U.S. Government is authorized to reproduce and distribute reprints for Government purposes notwithstanding any copyright notation thereon.

*Corresponding author. Tel.: +1 612 626 7781; fax: +1 612 625 4583.
E-mail addresses: xlluo@ece.umn.edu (X. Luo), georgios@ece.umn.edu (G.B. Giannakis).

0165-1684/$ - see front matter © 2006 Elsevier B.V. All rights reserved.
doi:10.1016/j.sigpro.2005.06.025

too can neither handle severe ISI nor multi-user interference (MUI). Utilizing the nonzero mean property of pulse position modulation (PPM), an algorithm for timing synchronization and channel estimation was introduced in [6] for single-user UWB links, but the required sampling rates can be prohibitively high.

In this paper, we build on our recent work in [7] where we put forth a blind low-complexity timing estimator which is resilient to ISI and MUI. Because it can be implemented in an analog fashion, it also bypasses the need for high sampling rates.

Following timing acquisition, two types of demodulators have been proposed to exploit the rich multipath diversity provided by UWB channels. The most prevalent one is the RAKE structure which unfortunately in the UWB setup has to rely on a large number of fingers to capture sufficient energy for reliable detection [8]. Furthermore, since a large number of finger delays and weights have to be estimated, estimation errors affect critically the performance of RAKE reception in practical UWB radios. In [9], the performance of RAKE with estimated tap weights is analyzed. Delay estimation errors in the RAKE are studied in [10] and [11], where pronounced sensitivity of the RAKE receiver to mistiming is quantified. Besides RAKE, another candidate for demodulating UWB transmissions is an autocorrelation based receiver, where the received signal is correlated with a self-derived noisy template generated from a pilot waveform (a.k.a. transmit reference) [12,13]. The transmit reference (TR) based demodulator collects the available multipath diversity without explicitly estimating the UWB channel, and is relatively robust to mistiming. However, it sacrifices data rate for transmitting the reference waveforms and does not allow for ISI. Also, the noise present in the noisy TR template may severely degrade the probability of detection error for the signal-to-noise-ratio (SNR) values of practical interest. In [14] and [15], comparisons between RAKE and TR receivers have been performed under specific system models. Enjoying full multipath diversity, the synchronized aggregate template (SAT) receiver proposed in [7] exhibits very attractive performance in the SNR range of practical interest. In this paper, to further expose the merits of SAT-based demodulation, we compare the SAT receiver with the traditional RAKE receiver analytically and by simulations from various perspectives including complexity, sensitivity to mistiming, and energy capture capability.

The rest of the paper is organized as follows. Section 2 describes the system model and states the problem we will address. Relying on properly designed nonzero mean UWB transmissions, Section 3 reviews the algorithms we derived in [7] for timing acquisition, SAT recovery, and SAT-based demodulation of binary pulse amplitude modulation (BPAM) before generalizing them to binary pulse position modulation (BPPM). In Section 4, we investigate the performance of our timing estimator, and in Section 5 we analyze the detection performance of the SAT-based demodulator. Section 6 compares SAT against RAKE, and Section 7 provides corroborating simulations. Finally, Section 8 concludes the paper.

2. System model and problem statement

Consider an ad hoc UWB network configuration as in Fig. 1, where node A is broadcasting bit stream $\{b(n)\}$ with period T_s. Node C, already synchronized to node A, is in the demodulation mode. Node B is a "new" node that wants to listen to node A's transmission and thus, as a first step, it needs to acquire timing synchronization with node A. Node A transmits information bits using either BPAM or BPPM, the two modulations typically used by UWB modems.

For BPAM, the transmitted signal from node A can be written as

$$u(t) = \sqrt{\mathscr{E}} \sum_n s(\lfloor n/N_f \rfloor) p(t - nT_f - c_n T_c), \qquad (1)$$

where $\mathscr{E}$ is the transmitted energy per pulse; $p(t)$ is the unit-energy monocycle: $\int_0^{T_p} p^2(t)\,dt = 1$; $c_n \in [0, N_c - 1]$ is the user specific time hopping (TH) code with N_c chips of duration T_c which enables multiple access (MA); $T_f = N_c T_c$ is the frame

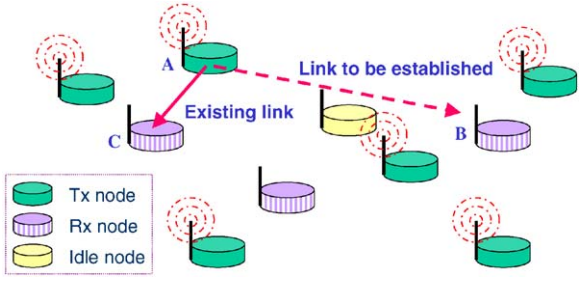

Fig. 1. A multi-access ad hoc configuration.

period, and $T_s = N_f T_f$ is the symbol (bit) period consisting of N_f frames; and $s(k) = 2b(k) - 1$ is the antipodal information bearing symbol, each transmitted over N_f frames (n in (1) is the frame index and $\lfloor\cdot\rfloor$ denotes integer floor). We choose the TH code to be N_f-periodic, i.e., $c_{n+N_f} = c_n$, in which case $u(t)$ in (1) can be simplified as

$$u(t) = \sqrt{\mathscr{E}} \sum_k s(k) p_T(t - kT_s), \tag{2}$$

where $p_T(t) := \sum_{n=0}^{N_f-1} p(t - nT_f - c_n T_c)$ is the transmit symbol waveform.

For BPPM, on the other hand, the transmitted signal can be expressed as

$$u(t) = \sqrt{\mathscr{E}} \sum_n a(\lfloor n/N_f \rfloor) p(t - nT_f - c_n T_c - b(\lfloor n/N_f \rfloor)\Delta), \tag{3}$$

where $a(k) = \pm 1$ is a sequence whose usefulness will become clear later; and Δ is the so-called modulation index. We select $\Delta > T_p$, where T_p denotes the duration of the monocycle $p(t)$. Again, for N_f-periodic TH codes, $u(t)$ in (3) reduces to

$$u(t) = \sqrt{\mathscr{E}} \sum_k a(k) p_T(t - kT_s - b(k)\Delta), \tag{4}$$

where $p_T(t)$ is defined as in (2).

The multipath channel between nodes A and B is modeled as a tap-delay line:

$$h(t) = \sum_{l=0}^{L} \alpha_l \delta(t - \tau_l), \tag{5}$$

with real path gains $\{\alpha_l\}_{l=0}^L$ and path delays $\{\tau_l\}_{l=0}^L$ assumed invariant over a block of symbols (block fading model). In a typical UWB propagation, the channel's coherence time (T_{coh}) satisfies: $T_{coh} \gg T_s$ [16]. Defining $\tau_{l,0} := \tau_l - \tau_0$, with τ_0 being the first path arrival time, the channel delay spread is just $\tau_{L,0}$. At the receiver, we can combine the channel and transmit-filter to form the receive symbol waveform $p_R(t) := p_T(t) \star h(t + \tau_0)$, where $\star$ stands for linear convolution. At each receiving node, we will observe $u(t) \star h(t)$ in the presence of multi-user interference (MUI) $\rho(t)$ and additive Gaussian nose (AGN) $\eta(t)$. The latter has two-sided power spectral density $N_0/2$ and bandwidth W dictated by the low-pass front-end filter's cutoff frequency. For BPAM transmissions as in (2), the received signal at node B is

$$r(t) = \sqrt{\mathscr{E}} \sum_n s(n) p_R(t - nT_s - \tau_0) + \rho(t) + \eta(t). \tag{6}$$

Similarly, for BPPM as in (4), we have

$$r(t) = \sqrt{\mathscr{E}} \sum_n a(n) p_R(t - nT_s - b(n)\Delta - \tau_0) + \rho(t) + \eta(t). \tag{7}$$

Node B receives $r(t)$ and wishes to find τ_0 (i.e., perform timing acquisition), and subsequently demodulate the information bits $b(n)$. The goal of this paper is twofold:

Design a transmission protocol to estimate τ_0 and $p_R(t)$ blindly, given only $r(t)$ in the presence of noise, MUI, and ISI. Furthermore, derive a low-complexity demodulation scheme that is robust to timing acquisition errors.

To address these objectives, we will adopt the following operating conditions:

C1. We choose the symbol period $T_s > \Delta\tau_{max} - T_T$, where $T_T := \sup\{t | p_T(t) \neq 0\}$ and $\Delta\tau_{max} \geqslant \max_{l\in[1,L]}(\tau_l - \tau_{l-1})$ denotes a known upper bound on successive path delay differences.

C2. With the delay spread $\tau_{L,0}$ (and thus $T_R := \sup\{t | p_R(t) \neq 0\} = T_T + \tau_{L,0}$) known, we select an integer $M := \lceil T_R/T_s \rceil + 1$.

C3. At any given time, there is only one node synchronizing other nodes by transmitting periodically nonzero mean signals, e.g., node A in Fig. 1.

Condition C1 ensures that over the $[0, T_R]$ support of $p_R(t)$, intervals where $p_R(t) = 0$ are no larger than T_s—a condition whose usefulness will become clear soon. For clarity in exposition, we rely on exact knowledge of $\tau_{L,0}$ in C2. But, as shown in [7], our ensuing results carry over even when only an upper bound of $\tau_{L,0}$ is available. Condition C3 will prove useful in suppressing MUI.

3. Timing and demodulation based on SAT

During the synchronization phase, we will periodically modify the signal transmitted from node A so that the signal received at node B has nonzero mean. This will be done without sacrificing data rate or interrupting the already established links (e.g., the link from node A to node C in Fig. 1). Node B will rely on this nonzero mean transmitted signal by node A to acquire timing and the synchronized aggregate template (SAT) $p_R(t)$. In the following two subsections, we will review the SAT recovery

algorithm we derived in [7] for BPAM, and we will generalize it to BPPM transmissions.

3.1. SAT for BPAM

Recall that for BPAM, $s(n)=2b(n)-1$ in (2) takes ± 1 values equiprobably, i.e., it is a zero-mean symmetric PAM (S-PAM). Our synchronization pattern will also rely on nonzero mean symbols drawn from an asymmetric PAM (A-PAM): $s(n)=2b(n)-1+2\theta\delta_{b(n),1}$, where $\theta>0$ and $\delta_{i,j}$ denotes Kronecker's delta, i.e., $\delta_{i,j}=0$ when $i\neq j$ and $\delta_{i,j}=1$ when $i=j$. When $b(n)=0$, the transmitted A-PAM symbol will be $s(n)=-1$; and when $b(n)=1$, we will transmit $s(n)=+1+2\theta$. Our idea for SAT recovery is to transmit A-PAM symbols during the synchronization phase with period M selected as in C2, i.e.,

$$s(kM)=2b(kM)-1+2\theta\delta_{b(kM),1},$$

$$s(kM+m)=2b(kM+m)-1,\quad m\in[1,M-1]. \tag{8}$$

It is worth stressing that signaling as in (8) does not affect the detector of those already synchronized users (e.g., node C in Fig. 1). Those users can continue their original detection process with improved BER because of the increased transmission energy. Upon completing the synchronization phase, the broadcasting node A will return to S-PAM to be energy efficient. Based on (8) and recalling C3, let us take expectation of the received signal in (6) to obtain

$$\mathsf{E}r(t)=\sqrt{\mathscr{E}}\theta\sum_k p_{\mathrm{R}}(t-kMT_s-\tau_0). \tag{9}$$

Because $\mathsf{E}r(t)$ is periodic with period MT_s, a natural estimator for one of its periods is

$$\bar{r}(t)=\frac{1}{N}\sum_{n=0}^{N-1} r(t+nMT_s),\quad t\in[0,MT_s], \tag{10}$$

where N is the number of averaged segments of $r(t)$. Relying on $\mathsf{E}r(t)$ (or $\bar{r}(t)$ in practice), condition C1 ensures that timing τ_0 can be acquired uniquely using [7]

$$\tau_0=\arg\max_{\tau\in[0,MT_s)} J(\tau), J(\tau):=\int_0^{T_{\mathrm{R}}}[\mathsf{E}r(t+\tau)]^2\,\mathrm{d}t. \tag{11}$$

Having acquired τ_0, we can recover the synchronized aggregate template $p_{\mathrm{R}}(t)$ as:

$$p_{\mathrm{R}}(t)=\frac{1}{\sqrt{\mathscr{E}}}\frac{1}{\theta}\mathsf{E}r(t+\tau_0),\quad t\in[0,T_{\mathrm{R}}]. \tag{12}$$

Using (10) to replace ensemble- with sample-mean in (11) and (12), we have established the following result in [7]:

Proposition 1. *Under* C1–C3, *with the periodic* A-PAM *pattern in* (8) *during the synchronization phase, the timing offset* τ_0 *and the* SAT $p_{\mathrm{R}}(t)$ *can be estimated blindly in the presence of* ISI *and* MUI *by using*

$$\hat{\tau}_0=\arg\max_{\tau\in[0,MT_s)}\int_0^{T_{\mathrm{R}}}\bar{r}^2((t+\tau)_{\mathrm{mod}\,MT_s})\,\mathrm{d}t,$$

$$\hat{p}_{\mathrm{R}}(t)=\frac{1}{\sqrt{\mathscr{E}}}\frac{1}{\theta}\bar{r}(t+\hat{\tau}_0),\quad t\in[0,T_{\mathrm{R}}], \tag{13}$$

where the (mod MT_s) *operation is used because* $\bar{r}(t)$ *in* (10) *is estimated over a period of size* MT_s *whereas the integration in* (13) *needs its periodic extension.*

In order to capture the full energy in $p_{\mathrm{R}}(t)$, when we have available $\hat{\tau}_0$ and $\hat{p}_{\mathrm{R}}(t)$, we demodulate using a SAT-based correlator. Specifically, we form the following decision statistic:

$$d(k)=\int_0^{T_{\mathrm{R}}}\hat{p}_{\mathrm{R}}(t)r(t+\hat{\tau}_0+kT_s)\,\mathrm{d}t. \tag{14}$$

When the amount of ISI is tolerable, we can simply demodulate the transmitted symbol with a sign detector: $\hat{s}(k)=\mathsf{sign}[d(k)]$. Otherwise, Viterbi's Algorithm (VA) can be applied to demodulate a sequence of symbols. In Sections 4 and 5, we will study in detail the performance of the timing estimator in (13) and the SAT-based sign detector.

3.2. SAT for BPPM

In the case of BPPM, after synchronization has been accomplished, we let each transmitting node use $a(k)=2X_k-1$ in (4) with $\{X_k\}$ being i.i.d. Bernoulli random variables taking 0, 1 values equiprobably. As a result, the mean of the transmitted signal from any node in normal communication phase has zero mean. Thus, the mean of the MUI $\rho(t)$ in (7) will be zero because we have assumed in C3 that except for node A no other nodes transmit nonzero mean signals. To enable synchronization with BPPM, node A selects $a(k)$ according to the following rule:

$$a(kM)=(2X_{kM}-1)(1-\delta_{b(kM),0})+\delta_{b(kM),0},$$

$$a(kM+m)=2X_{kM+m}-1,\quad m\in[1,M-1], \tag{15}$$

where as before $M = \lceil T_R/T_s \rceil + 1$. We can easily verify that $a(k)$ is now periodically nonzero mean, i.e.,

$$\begin{aligned}\mathsf{E}[a(kM)] = {} & \Pr(b(kM)=0)\mathsf{E}[a(kM)|b(kM)=0] \\ & + \Pr(b(kM)=1)\mathsf{E}[a(kM)|b(kM)=1] \\ = {} & \tfrac{1}{2},\end{aligned}$$

and $\mathsf{E}[a(kM+m)] = 0$, $\forall m \in [1, M-1]$. With this choice of $a(n)$, the mean of the received signal at node B is [c.f. (7)]:

$$\mathsf{E}r(t) = \frac{\sqrt{\mathscr{E}}}{2}\sum_k p_R(t - kMT_s - \tau_0). \tag{16}$$

Clearly, the timing τ_0 and the SAT $p_R(t)$ can be obtained the same way described by (13) in Proposition 1. Thus, we can summarize our result for BPPM in the following corollary:

Corollary 1. *When we signal with* BPPM *under* C1–C3, *and we select* $a(k)$ *as in* (15) *during the synchronization phase and* $a(k) = 2X_k - 1$ *outside the synchronization phase, where* $\{X_k\}$ *are i.i.d. Bernoulli random variables*: $\Pr(X_k = 0) = \Pr(X_k = 1) = \frac{1}{2}$, *the timing offset* τ_0 *and the* SAT $p_R(t)$ *can be estimated blindly in the presence of* ISI *and* MUI *using*

$$\hat{\tau}_0 = \arg\max_{\tau\in[0,MT_s)} \int_0^{T_R} \bar{r}^2((t+\tau)_{\mathrm{mod}\, MT_s})\,\mathrm{d}t,$$

$$\hat{p}_R(t) = \frac{2}{\sqrt{\mathscr{E}}}\bar{r}(t+\hat{\tau}_0), \quad t \in [0, T_R]. \tag{17}$$

Similarly, when we have available $\hat{\tau}_0$ and $\hat{p}_R(t)$, demodulation can be performed by using a SAT-based correlator. Specifically, to combat the random sign $a(k)$, we form the following decision statistic (binary case):

$$\begin{aligned} d(k) = {} & \left| \int_0^{T_R} \hat{p}_R(t) r(t + \hat{\tau}_0 + kT_s)\,\mathrm{d}t \right| \\ & - \left| \int_\Delta^{T_R+\Delta} \hat{p}_R(t-\Delta) r(t + \hat{\tau}_0 + kT_s)\,\mathrm{d}t \right|. \end{aligned} \tag{18}$$

When the amount of ISI is tolerable, we can simply demodulate the transmitted binary bit as: $\hat{b}(k) = (1 - \mathsf{sign}[d(k)])/2$.

4. Timing performance

In this and the ensuing section, we will analyze the performance of our blind timing and SAT-based demodulation algorithms. For succinctness, we will only consider BPAM. Although a major advantage of our SAT-based receiver is its ability to blindly acquire timing and capture the full multipath energy even in the presence of severe ISI and MUI [7], for clarity in this and the next section, we will focus on a point-to-point (or a broadcasting) link free of MUI and ISI. To ensure ISI-free operation, we null the last chip of the TH code (i.e., we set $c_{N_f-1} = 0$) and choose $T_f > T_p + \tau_{L,0}$. Notice that IFI is still allowed by this choice. With this operational scenario, we see $T_R < T_s$ in (6) and $M = 2$ as per C2. Furthermore, using (10), (8), and (6), we have that for $t \in [0, 2T_s]$,

$$\begin{aligned} \bar{r}(t) = {} & \frac{1}{N}\sum_{n=0}^{N-1} r(t + n2T_s) \\ = {} & \frac{1}{N}\sum_{n=0}^{N-1}\Bigg[\eta(t+n2T_s) + \sqrt{\mathscr{E}}\sum_k\sum_{m=0}^{1} \\ & s(2k+m)p_R(t-(2k+m)T_s - \tau_0 + n2T_s)\Bigg] \\ = {} & \frac{\sqrt{\mathscr{E}}}{N}\sum_{n=0}^{N-1}\sum_{k=n-1}^{n} s(2k)p_R(t+2(n-k)T_s - \tau_0) \\ & + \frac{\sqrt{\mathscr{E}}}{N}\sum_{n=0}^{N-1}\sum_{k=n-2}^{n} s(2k+1) \\ & \times p_R(t+(2(n-k)-1)T_s - \tau_0) \\ & + \frac{1}{N}\sum_{n=0}^{N-1}\eta(t+n2T_s) \\ = {} & \sqrt{\mathscr{E}}\bar{S}_0\sum_{l=0}^{1} p_R(t+2lT_s - \tau_0) + \bar{\eta}(t) \\ & + \sqrt{\mathscr{E}}\bar{S}_1\sum_{l=0}^{2} p_R(t+(2l-1)T_s - \tau_0), \end{aligned} \tag{19}$$

where $\bar{\eta}(t) := \sum_{n=0}^{N-1}\eta(t+2nT_s)/N$, and we have used that for $N \gg 1$, $\sum_{n=0}^{N-1} s(2(n-1)) \doteq \sum_{n=0}^{N-1} s(2(n)) := N\bar{S}_0$, and $\sum_{n=0}^{N-1} s(2(n-2)+1) \doteq \sum_{n=0}^{N-1} s(2(n-1)+1) \doteq \sum_{n=0}^{N-1} s(2n+1) := N\bar{S}_1$. Without loss of generality, we will henceforth assume $\tau_0 \in [0, T_s)$. For $t \in [0, 2T_s]$ and $\tau_0 \in [0, T_s)$, the sample average in (19) simplifies to

$$\begin{aligned} \bar{r}(t) = {} & \sqrt{\mathscr{E}}\bar{S}_0 p_R(t - \tau_0) + \bar{\eta}(t) \\ & + \sqrt{\mathscr{E}}\bar{S}_1\sum_{l=0}^{1} p_R(t+(2l-1)T_s - \tau_0). \end{aligned} \tag{20}$$

In the remainder of this section, we will analyze the performance of $\hat{\tau}_0$ in (13) based on the $\bar{r}(t)$ expressed as in (20). Since $M = 2$ in the ISI-free case, we can rewrite (13) as

$$\hat{\tau}_0 = \arg \max_{\tau\in[0,2T_s)} J(\tau); \tag{21}$$

$$J(\tau) \coloneqq \int_{\tau}^{\tau+T_R} \bar{r}^2((t)_{\mathrm{mod}\ 2T_s})\,\mathrm{d}t. \tag{22}$$

Because $\hat{\tau}_0$ in (21) is a nonlinear estimator, *finite-sample* variance analysis is impossible; and for this reason, we will resort to simulated performance analysis when N is relatively small (see Section 7). In this section, we will pursue local performance analysis of $\hat{\tau}_0$ when N is large enough such that $\hat{\tau}_0 = \arg\max J(\tau) = \arg\min_{\dot{J}(\tau)=0}|\tau-\tau_0|$, where $\dot{J}(\tau) \coloneqq \mathrm{d}J(\tau)/\mathrm{d}\tau$. To this end, we will rely on a first-order perturbation analysis [17]. For a positive parameter $\varepsilon > 0$ satisfying $\varepsilon < \min\{\tau_{1,0}, \tau_{L,0} - \tau_{L-1,0},\ T_p, T_s - T_R\}$, the aggregate waveform $p_R(t)$ is differentiable around the end points of its support; i.e., for $t \in (0,\varepsilon] \cup [T_R - \varepsilon, T_R)$. When N is sufficiently large so that $\hat{\tau}_0 \in [\tau_0 - \varepsilon, \tau_0 + \varepsilon]$, our objective function $J(\tau)$ over this interval can be expressed as [c.f. (20) and (22)]: for $\tau \in [\tau_0 - \varepsilon, \tau_0 + \varepsilon]$,

$$\begin{aligned} J(\tau) &= \int_{\tau}^{\tau+T_R} \bar{r}^2(t)\,\mathrm{d}t \\ &= \int_{\tau}^{\tau+T_R} (\sqrt{\mathscr{E}}\bar{S}_0 p_R(t-\tau_0) + \bar{\eta}(t))^2\,\mathrm{d}t. \end{aligned} \tag{23}$$

For $\hat{\tau}_0 \in [\tau_0, \tau_0 + \varepsilon]$, we can write $\hat{\tau}_0 = \tau_0 + \Delta\tau$, and invoke the *mean value theorem* to express the derivative of $J(\tau)$ around τ_0 as

$$\dot{J}(\hat{\tau}_0) = \dot{J}(\tau_0 + \Delta\tau) = \dot{J}(\tau_0) + \ddot{J}(\tau_0 + \mu\Delta\tau)\Delta\tau, \tag{24}$$

where $\mu \in (0,1)$ is a function of $\Delta\tau$. Since $\dot{J}(\hat{\tau}_0) = 0$, we obtain

$$\Delta\tau = -\frac{\dot{J}(\tau_0)}{\ddot{J}(\tau_0 + \mu\Delta\tau)}. \tag{25}$$

When $\tau \in [\tau_0, \tau_0 + \varepsilon]$, we obtain from (23):

$$\begin{aligned} \dot{J}(\tau) = &-\mathscr{E}\bar{S}_0^2 p_R^2(\tau-\tau_0) - 2\sqrt{\mathscr{E}}\bar{S}_0 p_R(\tau-\tau_0)\bar{\eta}(\tau) \\ &+ \bar{\eta}^2(\tau+T_R) - \bar{\eta}^2(\tau), \end{aligned} \tag{26}$$

and after differentiating once more, we have

$$\begin{aligned} \ddot{J}(\tau) = &-2\mathscr{E}\bar{S}_0^2 p_R(\tau-\tau_0)\dot{p}_R(\tau-\tau_0) \\ &- 2\sqrt{\mathscr{E}}\bar{S}_0[\dot{p}_R(\tau-\tau_0)\bar{\eta}(\tau) + p_R(\tau-\tau_0)\dot{\bar{\eta}}(\tau)] \\ &+ 2\bar{\eta}(\tau+T_R)\dot{\bar{\eta}}(\tau+T_R) - 2\bar{\eta}(\tau)\dot{\bar{\eta}}(\tau). \end{aligned} \tag{27}$$

For sufficiently large N, the noise related terms in (27) decrease at least as $O(1/N)$, which allows us to approximate $\ddot{J}(\tau)$ by its nonzero expectation $\mathsf{E}[\ddot{J}(\tau)]$; i.e.,

$$\begin{aligned} \ddot{J}(\tau) \doteq \mathsf{E}[\ddot{J}(\tau)] &= -2\mathscr{E}\theta^2 p_R(\tau-\tau_0)\dot{p}_R(\tau-\tau_0), \\ &\tau \in [\tau_0, \tau_0 + \varepsilon]. \end{aligned} \tag{28}$$

With this approximation, we can re-write (25) as

$$\begin{aligned} \Delta\tau &\doteq \frac{\dot{J}(\tau_0)}{2\mathscr{E}\theta^2 p_R(\mu\Delta\tau)\dot{p}_R(\mu\Delta\tau)} \\ &= \frac{\bar{\eta}^2(\tau_0+T_R) - \bar{\eta}^2(\tau_0)}{2\mathscr{E}\theta^2 p_R(\mu\Delta\tau)\dot{p}_R(\mu\Delta\tau)}. \end{aligned} \tag{29}$$

From (29), we can draw the following conclusions:

(1) If within the interval $[0,+\varepsilon]$, $p_R(t)$ behaves like $p_R(t) = t^a$ with $a > \frac{1}{2}$, then we have $p_R(t)\dot{p}_R(t) = at^{2a-1}$, which goes to zero as $t \to 0$. This leads to magnification of the timing estimation error since

$$p_R(\mu\Delta\tau)\dot{p}_R(\mu\Delta\tau) = a(\mu\Delta\tau)^{2a-1} \leqslant p_R(\varepsilon)\dot{p}_R(\varepsilon), \tag{30}$$

and from (29), we deduce that

$$\Delta\tau \geqslant \frac{\dot{J}(\tau_0)}{2\mathscr{E}\theta^2 p_R(\varepsilon)\dot{p}_R(\varepsilon)}. \tag{31}$$

The message here is that this kind of pulse shapers will not offer accurate timing estimates when N is large.

(2) If within interval $[0,+\varepsilon]$, $p_R(t)$ behaves like $p_R(t) = t^a$ with $a < \frac{1}{2}$, then we have $p_R(t)\dot{p}_R(t) = at^{2a-1} \to \infty$ as $t \to 0$. Thus, from (29) and unlike (31), we have

$$\Delta\tau \leqslant \frac{\dot{J}(\tau_0)}{2\mathscr{E}\theta^2 p_R(\varepsilon)\dot{p}_R(\varepsilon)}. \tag{32}$$

The message here is that when $p_R(t)$ behaves close to its endpoints like t^a with $a < \frac{1}{2}$, the timing estimator will exhibit low variance for N sufficiently large. To ensure that $p_R(t)$ behaves this way, we need to select the monocycle $p(t)$ properly. To this end, we choose $p(t)$ to satisfy the following endpoint properties (see also Fig. 2):

P1 (*Local behavior around* $t = 0$): $p(t) \propto t^a$ with $a < \frac{1}{2}$, $t \in [0,+\varepsilon]$;

P2 (*Local behavior around* $t = T_p$): $p(t) \propto (T_p - t)^b$ with $b < \frac{1}{2}$, $t \in [T_p - \varepsilon, T_p]$;

where ε is a parameter that is chosen to satisfy $0 < \varepsilon < \min\{\tau_{1,0}, \tau_{L,0} - \tau_{L-1,0}, T_p, T_s - T_R\}$.

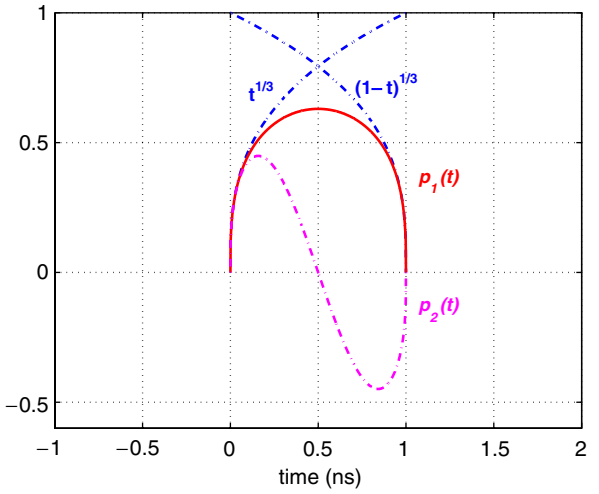

Fig. 2. Pulse shaper with preferred properties for accurate timing acquisition.

With this type of pulse shapers, we obtain from (32)

$$\begin{aligned}&\mathsf{E}[\Delta\tau^2|\Delta\tau\in[0,\varepsilon]]\\&\leqslant\frac{\mathsf{E}[\dot{J}^2(\tau_0)|\Delta\tau\in[0,\varepsilon]]}{4\mathscr{E}^2\theta^4p_{\mathrm{R}}^2(\varepsilon)\dot{p}_{\mathrm{R}}^2(\varepsilon)}\\&=\frac{\mathsf{E}[(\bar{\eta}^2(\tau_0+T_{\mathrm{R}})-\bar{\eta}^2(\tau_0))^2|\Delta\tau\in[0,\varepsilon]]}{4\mathscr{E}^2\theta^4p_{\mathrm{R}}^2(\varepsilon)\dot{p}_{\mathrm{R}}^2(\varepsilon)}\\&=\frac{N_0^2W^2}{N^2\mathscr{E}^2\theta^4p_{\mathrm{R}}^2(\varepsilon)\dot{p}_{\mathrm{R}}^2(\varepsilon)},\end{aligned}\tag{33}$$

where in establishing the last equality, we used the fact that for a zero-mean Gaussian random variable X, it holds that $\mathsf{E}[X^4]=3(\mathsf{E}[X^2])^2$.

Based on (33), we can finalize our local mean square error analysis of $\hat{\tau}_0$ as follows:

Proposition 2. *If $p(t)$ is selected to satisfy* P1 *and* P2, *as $N\to+\infty$, the mean square error in the timing estimator*: $\hat{\tau}_0=\arg\max_{\tau\in[0,2T_s]}\int_{\tau}^{\tau+T_{\mathrm{R}}}\bar{r}^2(t)\,\mathrm{d}t$ *is upper bounded by*

$$\begin{aligned}&\mathsf{E}[\Delta\tau^2]\\&\leqslant\frac{N_0^2W^2}{N^2\mathscr{E}^2\theta^4}\\&\quad\times\frac{1}{\min\{p_{\mathrm{R}}^2(\varepsilon)\dot{p}_{\mathrm{R}}^2(\varepsilon),p_{\mathrm{R}}^2(T_{\mathrm{R}}-\varepsilon)\dot{p}_{\mathrm{R}}^2(T_{\mathrm{R}}-\varepsilon)\}}.\end{aligned}\tag{34}$$

Proof. When N is large enough, $\hat{\tau}_0$ in (21) will lie in the interval $[\tau_0-\varepsilon,\tau_0+\varepsilon]$ with probability close to 1. Thus, we can write

$$\begin{aligned}&\mathsf{E}[\Delta\tau^2]\\&=\Pr(\Delta\tau\in[0,+\varepsilon])\mathsf{E}[\Delta\tau^2|\Delta\tau\in[0,+\varepsilon]]\\&\quad+\Pr(\Delta\tau\in[-\varepsilon,0])\mathsf{E}[\Delta\tau^2|\Delta\tau\in[-\varepsilon,0]]\\&\leqslant\Pr(\Delta\tau\in[0,+\varepsilon])\frac{N_0^2W^2}{N^2\theta^4\mathscr{E}^2p_{\mathrm{R}}^2(\varepsilon)\dot{p}_{\mathrm{R}}^2(\varepsilon)}\\&\quad+\Pr(\Delta\tau\in[-\varepsilon,0])\frac{N_0^2W^2}{N^2\theta^4\mathscr{E}^2p_{\mathrm{R}}^2(T_{\mathrm{R}}-\varepsilon)\dot{p}_{\mathrm{R}}^2(T_{\mathrm{R}}-\varepsilon)}\\&\leqslant\frac{N_0^2W^2}{N^2\mathscr{E}^2\theta^4}\frac{1}{\min\{p_{\mathrm{R}}^2(\varepsilon)\dot{p}_{\mathrm{R}}^2(\varepsilon),p_{\mathrm{R}}^2(T_{\mathrm{R}}-\varepsilon)\dot{p}_{\mathrm{R}}^2(T_{\mathrm{R}}-\varepsilon)\}}.\end{aligned}$$

In the derivation, we have utilized the upper bound on $\mathsf{E}[\Delta\tau^2]$ conditioned upon $\Delta\tau\in[-\varepsilon,0]$, which can be easily obtained through straightforward manipulation of Eq. (26). □

Notice that although the mean-square error bound grows with W, which is huge in UWB transmissions, Proposition 1 establishes that by judiciously selecting the monocycle $p(t)$, we can ensure that the convergence rate of our mean square sense consistent timing estimator in (21) will be $\mathrm{O}(1/N^2)$. Besides increasing the amount of averaging N to lower the bound, in (34) we can reduce the mean-square error of our timing estimator by increasing the size of our periodically transmitted nonzero mean symbols θ. In Section 7, simulations will be carried out to test the proposed timing estimator's performance with relatively small N.

5. Detection performance of SAT

In this section, we will evaluate the performance of our SAT demodulator assuming that N is sufficiently large to guarantee that $\hat{\tau}_0$ is within T_s off the true τ_0, i.e., $|\tau_0-\hat{\tau}_0|<T_s$. Under this condition, we will estimate the SAT as $\hat{p}_{\mathrm{R}}(t)=\bar{r}(t+\hat{\tau}_0)/(\sqrt{\mathscr{E}}\theta)$ and then detect the transmitted symbol as described in Section 3 using

$$\begin{aligned}\hat{s}(k)&=\mathsf{sign}[d(k)]\\&=\mathsf{sign}\left[\int_0^{T_{\mathrm{R}}}\hat{p}_{\mathrm{R}}(t)r(t+\hat{\tau}_0+kT_s)\,\mathrm{d}t\right].\end{aligned}\tag{35}$$

Supposing temporarily that $\hat{\tau}_0\leqslant\tau_0$, we can express the SAT estimate as [c.f. (20)]:

$$\begin{aligned}\hat{p}_{\mathrm{R}}(t)=&\frac{\bar{S}_0}{\theta}p_{\mathrm{R}}(t-\tilde{\tau}_0)+\frac{\bar{S}_1}{\theta}p_{\mathrm{R}}(t+T_s-\tilde{\tau}_0)\\&+\frac{1}{\sqrt{\mathscr{E}}\theta}\bar{\eta}(t+\hat{\tau}_0),\quad t\in[0,T_{\mathrm{R}}],\end{aligned}\tag{36}$$

where $\tilde{\tau}_0 := \tau_0 - \hat{\tau}_0$. Substituting (36) into (35), we have

$$\begin{aligned} d(k) &= \int_0^{T_R} \hat{p}_R(t)\eta(t+\hat{\tau}_0+kT_s)\,dt + \sqrt{\mathscr{E}} \\ &\quad \times \int_0^{T_R} \hat{p}_R(t)\sum_n s(n) \\ &\quad \times p_R(t-nT_s-\tau_0+\hat{\tau}_0+kT_s)\,dt \end{aligned}$$

$$\begin{aligned} &= \eta_k + \sqrt{\mathscr{E}}\frac{\bar{S}_0}{\theta}E_C(\tilde{\tau}_0)s(k) + \frac{s(k)\bar{\eta}+s(k-1)\bar{\eta}_-}{\theta} \\ &\quad + \sqrt{\mathscr{E}}\frac{\bar{S}_1}{\theta}E_C(\tilde{\tau}_0-T_s)s(k-1), \end{aligned} \tag{37}$$

where $\eta_k := \int_0^{T_R} \hat{p}_R(t)\eta(t+kT_s+\hat{\tau}_0)\,dt$, $E_C(u) := \int_0^{T_R} p_R^2(t-u)\,dt$, $\bar{\eta} := \int_0^{T_R} \bar{\eta}(t+\hat{\tau}_0)p_R(t-\tilde{\tau}_0)\,dt$, and $\bar{\eta}_- := \int_0^{T_R} \bar{\eta}(t+\hat{\tau}_0)p_R(t+T_s-\tilde{\tau}_0)\,dt$.

To analyze the performance of the detector (35) based on (37), let us note first that

$$\mathsf{E}[\bar{S}_0] = \theta, \quad \mathsf{Var}(\bar{S}_0) = \frac{(\theta+1)^2}{N},$$

$$\mathsf{E}[\bar{S}_1] = 0, \quad \mathsf{Var}(\bar{S}_1) = \frac{1}{N};$$

$$\mathsf{E}[\bar{\eta}] = 0, \quad \mathsf{Var}(\bar{\eta}) = \frac{N_0}{2N}E_C(\tilde{\tau}_0),$$

$$\mathsf{E}[\bar{\eta}_-] = 0, \quad \mathsf{Var}(\bar{\eta}_-) = \frac{N_0}{2N}E_C(\tilde{\tau}_0-T_s).$$

Clearly, the random variable η_k has zero mean and variance:

$$\begin{aligned} \mathsf{E}[\eta_k^2] &= \mathsf{E}[\mathsf{E}[\eta_k^2|\bar{S}_0,\bar{S}_1,\bar{\eta}(t)]] \\ &= \mathsf{E}\left[\frac{N_0}{2}\int_0^{T_R}\hat{p}_R^2(t)\,dt\right] \\ &= \frac{\theta^2+(\theta+1)^2/N}{\theta^2}E_C(\tilde{\tau}_0) + \frac{1}{N\theta^2}E_C(\tilde{\tau}_0-T_s) \\ &\quad + \frac{N_0WT_R}{\mathscr{E}N\theta^2}. \end{aligned} \tag{38}$$

The average signal-to-interference-plus-noise-ratio (SINR) in (37) is then given by (39). For large enough N, (39) can be simplified to

$$\begin{aligned} &\mathrm{SINR}_{\mathrm{SAT}} \\ &= \frac{\mathsf{E}[(\sqrt{\mathscr{E}}(\bar{S}_0/\theta)E_C(\tilde{\tau}_0)s(k)+(1/\theta)s(k)\bar{\eta})^2]}{\mathsf{E}[(\sqrt{\mathscr{E}}(\bar{S}_1/\theta)E_C(\tilde{\tau}_0-T_s)s(k-1)+(1/\theta)s(k-1)\bar{\eta}_-+\eta_k)^2]} \\ &= \frac{\mathsf{E}[\mathscr{E}(\bar{S}_0^2/\theta^2)E_C^2(\tilde{\tau}_0)s^2(k)]+\mathsf{E}[(s^2(k)/\theta^2)\bar{\eta}^2]}{\mathsf{E}[\mathscr{E}(\bar{S}_1^2/\theta^2)E_C^2(\tilde{\tau}_0-T_s)s^2(k-1)]+\mathsf{E}[(s^2(k-1)/\theta^2)\bar{\eta}_-^2]+\mathsf{E}[\eta_k^2]} \\ &= \frac{\mathscr{E}(1+((\theta+1)^2/N\theta^2))E_C^2(\tilde{\tau}_0)+(N_0E_C(\tilde{\tau}_0)/2N\theta^2)}{(N_0/2)(1+((\theta+1)^2/N\theta^2))E_C(\tilde{\tau}_0)+(WT_RN_0^2/2N\theta^2\mathscr{E})+\mathscr{E}(E_C^2(\tilde{\tau}_0-T_s)/N\theta^2)+(N_0E_C(\tilde{\tau}_0-T_s)/N\theta^2)}. \end{aligned} \tag{39}$$

$$\begin{aligned} \mathrm{SINR}_{\mathrm{SAT}} &\doteq \frac{\mathscr{E}E_C^2(\tilde{\tau}_0)}{(N_0/2)E_C(\tilde{\tau}_0)+(WT_RN_0^2/2N\theta^2\mathscr{E})} \\ &= \frac{2\mathscr{E}E_C(\tilde{\tau}_0)}{N_0}\left(1+\frac{WT_R}{N\theta^2}\frac{N_0}{\mathscr{E}E_C(\tilde{\tau}_0)}\right)^{-1}, \end{aligned} \tag{40}$$

which leads to the following approximate expression for the probability of error of the detector in (35):

$$\begin{aligned} P_e^{\mathrm{SAT}} &\doteq Q(\sqrt{\mathrm{SINR}_{\mathrm{SAT}}}) \\ &= Q\left(\sqrt{\frac{2\mathscr{E}E_C(\tilde{\tau}_0)}{N_0}}\left(1+\frac{WT_R}{N\theta^2}\frac{N_0}{\mathscr{E}E_C(\tilde{\tau}_0)}\right)^{-1/2}\right). \end{aligned} \tag{41}$$

Now, we can summarize our result on SAT-based demodulation in the following proposition:

Proposition 3. *For a point-to-point link without* ISI, *when the timing estimate* $\hat{\tau}_0$ *incurs error* $\tilde{\tau}_0 := \tau_0 - \hat{\tau}_0$ *bounded by one symbol period* T_s, *i.e.*, $|\tilde{\tau}_0| < T_s$, *as the number of samples* N *in* (10) *grows large, the asymptotic* SINR *of the* SAT*-based detector in* (35) *is given by* (40) *and correspondingly the asymptotic* BER *by* (41).

Because the only term in (40) affected by timing error is $E_C(\tilde{\tau}_0) = \int_0^{T_R} p_R^2(t-\tau_0+\hat{\tau}_0)\,dt$, the SAT receiver exhibits robustness to mistiming so long as $E_C(\tilde{\tau}_0)$ is sufficiently large. Indeed, $E_C(\tilde{\tau}_0)$ matters more than the accuracy of $\hat{\tau}_0$. Even when the error

$\tilde{\tau}_0$ is relatively high, if E_C captures most of the multipath-spread energy, the resultant BER will be low; see also [11]. This is important since after all the goal is reliable demodulation rather than "super-accurate" synchronization. In Section 7, we will verify through simulations that the expression for the asymptotic probability of detection error in (41) is accurate enough and predicts well the dependence of P_e^{SAT} on N.

6. SAT vs. RAKE

In UWB communications, the RAKE receiver is typically employed to collect the ample multipath-induced energy. If perfect knowledge of $\{\tau_l\}_{l=0}^{L}$ in (5) is available, the RAKE receiver with L_r diversity branches will select $\{\tau_{l,0}\}_{l\in I_{L_r}}$ as branch delays, where I_{L_r} is the selected path index set, and then perform maximum ratio combining (MRC) of the L_r branch outputs $\{\int_0^{T_s} p_{\mathrm{T}}(t-\tau_{l,0})r(t+kT_s+\tau_0)\,\mathrm{d}t\}_{l\in I_{L_r}}$. In the following two subsections, we will compare our SAT receiver with the RAKE receiver from various aspects. Again, to prevent ISI at the receiver, i.e., in order to ensure that $T_{\mathrm{R}} < T_s$, we let $c_{N_{\mathrm{f}}-1} = 0$ and select T_{f} such that $T_{\mathrm{f}} > \tau_{L,0} + T_p$.

6.1. Ideal SAT vs. ideal RAKE

As $N \to \infty$ in (10), the law of large numbers implies that $\bar{r}(t)$ will converge to $\mathsf{E}r(t)$ in the mean square sense. Thus, our timing estimate $\hat{\tau}_0$ and recovered SAT $\hat{p}_{\mathrm{R}}(t)$ in (13) will converge to τ_0 and $p_{\mathrm{R}}(t)$, respectively. The ideal SAT receiver is the one based on perfect $p_{\mathrm{R}}(t)$ knowledge. With perfect SAT, the decision statistic in (14) becomes

$$d_{\mathrm{SAT}}(k) = s(k)\sqrt{\mathscr{E}}\int_0^{T_{\mathrm{R}}} p_{\mathrm{R}}^2(t)\,\mathrm{d}t + \int_0^{T_{\mathrm{R}}} \eta(t+\tau_0+kT_s)p_{\mathrm{R}}(t)\,\mathrm{d}t, \tag{42}$$

which is exactly the sampled value of the output of the filter with impulse response $p_{\mathrm{R}}(T_{\mathrm{R}}-t)$ matched to the receive symbol waveform $p_{\mathrm{R}}(t)$.

For the RAKE receiver with L_r fingers, when the optimal combining coefficients are $\{\check{\alpha}_l\}_{l\in I_{L_r}}$, the resulting decision statistic is

$$\begin{aligned} d_{\mathrm{RAKE}}(k) &= \sum_{l\in I_{L_r}} \check{\alpha}_l \int_0^{T_s} p_{\mathrm{T}}(t-\tau_{l,0})r(t+kT_s+\tau_0)\,\mathrm{d}t \\ &= \int_0^{T_s} \sum_{l\in I_{L_r}} \check{\alpha}_l p_{\mathrm{T}}(t-\tau_{l,0})r(t+kT_s+\tau_0)\,\mathrm{d}t \\ &= s(k)\sqrt{\mathscr{E}}\int_0^{T_s} \check{p}_{\mathrm{R}}(t)p_{\mathrm{R}}(t)\,\mathrm{d}t \\ &\quad + \int_0^{T_s} \check{p}_{\mathrm{R}}(t)\eta(t+kT_s+\tau_0)\,\mathrm{d}t, \end{aligned} \tag{43}$$

where $\check{p}_{\mathrm{R}}(t) := \sum_{l\in I_{L_r}} \check{\alpha}_l p_{\mathrm{T}}(t-\tau_{l,0})$. Clearly, $d_{\mathrm{RAKE}}(k)$ is the sampled output of a filter with impulse response $\check{p}_{\mathrm{R}}(T_s-t)$. Since it is well known that the SNR at the matched filter output is maximum [18], we have the following result:

Proposition 4. *For a single-user link without* ISI, *as* $N \to +\infty$, *the* SAT *receiver yields the maximum* SNR *at its output. In order to catch up with it, the* RAKE *receiver needs to employ as many fingers as the number of paths in the channel, i.e.,* $L_r \to L+1$; *see* (5). *Meanwhile, the* RAKE *requires perfect knowledge of* $p_{\mathrm{T}}(t)$, *and ideal estimates of the* $\{\tau_l, \alpha_l\}_{l=0}^{L}$ *channel parameters—none of which is required by the* SAT *receiver.*

6.2. Practical SAT vs. practical RAKE

In order to analytically characterize the performance of the RAKE in a single-user link without ISI, we henceforth also assume equi-spaced path delays $\tau_{l,0} = lT_\Omega$, where T_Ω dictates the resolution. Here, we further take $T_\Omega > T_p$, where T_p is the time duration of the monocycle $p(t)$. Since RAKE assumes knowledge of the TH code in (2) and (6), to balance the comparison with SAT, we neglect the TH code and re-write the transmit symbol waveform as: $p_{\mathrm{T}}(t) = \sum_{n=0}^{N_{\mathrm{f}}-1} p(t-nT_{\mathrm{f}})$; and the receive symbol waveform as: $p_{\mathrm{R}}(t) = \sum_{n=0}^{N_{\mathrm{f}}-1}\sum_{l=0}^{L}\alpha_l p(t-lT_\Omega-nT_{\mathrm{f}})$. As before, selecting $T_{\mathrm{f}} > T_p + LT_\Omega$ prevents ISI. Thus, we have $E_{\mathrm{C}}(0) = \int p_{\mathrm{R}}^2(t)\,\mathrm{d}t = E_{\mathrm{T}}\sum_{l=0}^{L}\alpha_l^2$, where $E_{\mathrm{T}} := \int p_{\mathrm{T}}^2(t)\,\mathrm{d}t$.

From the SINR expression in (40), we know how the SAT receiver gains robustness to timing errors and is effective in collecting the multipath energy. In contrast, the RAKE receiver is known to be particularly sensitive to timing errors and the multipath energy collected tends to diminish even when mis-timing is in the order of T_p [11]. In the remaining part of this section, we will assume that perfect timing information is available for the RAKE receiver. The only parameters that must be estimated are those MRC coefficients, which turn

out to be just the corresponding path gains $\{\alpha_l\}_{l=0}^{L}$ here.

With L_r fingers in the RAKE, let I_{L_r} be the set of selected path indices and $\{iT_\Omega\}_{i\in I_{L_r}}$ denote the branch delays. The optimal combining coefficients $\{\alpha_i\}_{i\in I_{L_r}}$ can be estimated by transmitting N training symbols; e.g., using $s(k)=1, k=0,1,\ldots,N-1$ in (6) allows one to recover the SAT as

$$\begin{aligned}\hat{p}_{\mathrm{R}}(t) &= \frac{1}{\sqrt{\mathscr{E}}}\frac{1}{N}\sum_{k=0}^{N-1} r(t+\tau_0+kT_s)\\ &= p_{\mathrm{R}}(t)+\frac{1}{\sqrt{\mathscr{E}}}\bar{\eta}(t+\tau_0).\end{aligned} \tag{44}$$

The combining coefficients can then be estimated using the maximum likelihood approach [14]

$$\begin{aligned}\hat{\alpha}_i &= \frac{1}{E_{\mathrm{T}}}\int_0^{T_{\mathrm{R}}} \hat{p}_{\mathrm{R}}(t)p_{\mathrm{T}}(t-iT_\Omega)\,\mathrm{d}t\\ &= \alpha_i+\frac{1}{\sqrt{\mathscr{E}}E_{\mathrm{T}}}\int_0^{T_{\mathrm{R}}}\bar{\eta}(t+\tau_0)p_{\mathrm{T}}(t-iT_\Omega).\end{aligned} \tag{45}$$

Because $\bar{\eta}(t):=\sum_{n=0}^{N-1}\eta(t+nT_s)/N$, we find that $\int_0^{T_{\mathrm{R}}}\bar{\eta}(t+\tau_0)p_{\mathrm{T}}(t-iT_\Omega)$ is zero mean Gaussian with variance $N_0E_{\mathrm{T}}/(2N)$. So we have

$$\mathsf{E}[\hat{\alpha}_i]=\alpha_i,\quad \mathsf{Var}(\hat{\alpha}_i)=\frac{N_0}{\mathscr{E}E_{\mathrm{T}}}\frac{1}{2N}. \tag{46}$$

The RAKE receiver will rely on the template:

$$\hat{h}(t)=\sum_{i\in I_{L_r}}\hat{\alpha}_i p_{\mathrm{T}}(t-iT_\Omega), \tag{47}$$

to correlate with $r(t)$ and yield at its output the following decision statistic:

$$\begin{aligned}d_{\mathrm{RAKE}}(k) &= \int_0^{T_s}\hat{h}(t)r(t+kT_s+\tau_0)\,\mathrm{d}t\\ &= s(k)\sqrt{\mathscr{E}}\int_0^{T_s}p_{\mathrm{R}}(t)\hat{h}(t)\,\mathrm{d}t\\ &\quad+\int_0^{T_s}\eta(t+kT_s+\tau_0)\hat{h}(t)\,\mathrm{d}t\\ &= s(k)\sqrt{\mathscr{E}}E_{\mathrm{T}}\sum_{i\in I_{L_r}}\alpha_i\hat{\alpha}_i+\sum_{i\in I_{L_r}}\hat{\alpha}_i\eta_{k,i},\end{aligned} \tag{48}$$

where $\eta_{k,i}:=\int_0^{T_s}p_{\mathrm{T}}(t-iT_\Omega)\eta(t+kT_s+\tau_0)\,\mathrm{d}t$ are i.i.d. zero-mean Gaussian with variance $N_0E_{\mathrm{T}}/2$. The average SNR in (48) is

$$\begin{aligned}&\mathrm{SNR}_{\mathrm{RAKE}}\\ &=\frac{\mathsf{E}[(s(k)\sqrt{\mathscr{E}}E_{\mathrm{T}}\sum_{i\in I_{L_r}}\alpha_i\hat{\alpha}_i)^2]}{\mathsf{E}[(\sum_{i\in I_{L_r}}\hat{\alpha}_i\eta_{k,i})^2]}\\ &=\frac{\mathscr{E}E_{\mathrm{T}}^2(\sum_{i\in I_{L_r}}\alpha_i^2)^2+\mathscr{E}E_{\mathrm{T}}^2(\sum_{i\in I_{L_r}}\alpha_i^2)(N_0/\mathscr{E}E_{\mathrm{T}})(1/2N)}{\sum_{i\in I_{L_r}}(\alpha_i^2+(N_0/\mathscr{E}E_{\mathrm{T}})(1/2N))(N_0E_{\mathrm{T}}/2)}.\end{aligned} \tag{49}$$

For N large enough, we can approximate (49) with:

$$\begin{aligned}&\mathrm{SNR}_{\mathrm{RAKE}}\\ &\doteq\frac{\mathscr{E}E_{\mathrm{T}}^2(\sum_{i\in I_{L_r}}\alpha_i^2)^2}{(\sum_{i\in I_{L_r}}\alpha_i^2)(N_0E_{\mathrm{T}}/2)+(L_r/4N)(N_0^2/\mathscr{E})}\\ &=\frac{2\mathscr{E}E_{\mathrm{T}}\sum_{i\in I_{L_r}}\alpha_i^2}{N_0}\left(1+\frac{L_r}{2N}\frac{N_0}{\mathscr{E}E_{\mathrm{T}}\sum_{i\in I_{L_r}}\alpha_i^2}\right)^{-1}.\end{aligned} \tag{50}$$

Using (50), the probability of detection error of the sign detector: $\hat{s}(k)=\mathsf{sign}[d_{\mathrm{RAKE}}(k)]$ can be approximated by the following expression:

$$\begin{aligned}&P_e^{\mathrm{RAKE}}\\ &\doteq Q\left(\sqrt{\mathrm{SNR}_{\mathrm{RAKE}}}\right)\\ &=Q\left(\sqrt{\frac{2\mathscr{E}E_{\mathrm{T}}\sum_{i\in I_{L_r}}\alpha_i^2}{N_0}}\right.\\ &\quad\left.\times\left(1+\frac{L_r}{2N}\frac{N_0}{\mathscr{E}E_{\mathrm{T}}\sum_{i\in I_{L_r}}\alpha_i^2}\right)^{-1/2}\right).\end{aligned} \tag{51}$$

Summarizing, the performance of the RAKE receiver can be characterized as follows:

Proposition 5. *Consider a single user link without* ISI *and channel model* $h(t)=\sum_{l=0}^{L}\alpha_l\delta(t-lT_\Omega-\tau_0)$ *with* $T_\Omega>T_p$. *Assuming perfect knowledge of* τ_0 *and* T_Ω, *the* RAKE *receiver with* L_r *branches having delays* $\{iT_\Omega\}_{i\in I_{L_r}}$ *and combining coefficients estimated as in* (45) *exhibits asymptotic* SNR (*as* $N\to\infty$) *given by* (50).

Substituting $\tilde{\tau}_0=0$ in (40), we can also obtain the following asymptotic SNR of the SAT receiver with perfect timing:

$$\begin{aligned}\mathrm{SNR}_{\mathrm{SAT}} &\doteq \frac{2\mathscr{E}E_{\mathrm{C}}(0)}{N_0}\left(1+\frac{WT_{\mathrm{R}}}{N_{\mathrm{SAT}}\theta^2}\frac{N_0}{\mathscr{E}E_{\mathrm{C}}(0)}\right)^{-1}\\ &= \frac{2\mathscr{E}E_{\mathrm{T}}\sum_{i=0}^{L}\alpha_i^2}{N_0}\\ &\quad\times\left(1+\frac{WT_{\mathrm{R}}}{N_{\mathrm{SAT}}\theta^2}\frac{N_0}{\mathscr{E}E_{\mathrm{T}}\sum_{i=0}^{L}\alpha_i^2}\right)^{-1},\end{aligned} \tag{52}$$

where N_{SAT} is the sample size used in (19) to form the average: $\bar{r}(t)$.

If we define the energy capture fraction of the RAKE receiver as: $\rho := (\sum_{i\in I_{L_r}} \alpha_i^2)/(\sum_{i=0}^{L} \alpha_i^2)$, we can write the asymptotic SNR of the RAKE receiver as [c.f. (50)]:

$$\mathrm{SNR}_{\mathrm{RAKE}} \doteq \frac{2\mathscr{E}E_{\mathrm{T}}\sum_{i=0}^{L}\alpha_i^2}{N_0} \times \left(1+\frac{L_r}{2N_{\mathrm{RAKE}}}\frac{N_0}{\mathscr{E}E_{\mathrm{T}}\sum_{i=0}^{L}\alpha_i^2\rho}\right)^{-1}\rho, \tag{53}$$

where N_{RAKE} is the number of samples used to obtain $\hat{p}_{\mathrm{R}}(t)$ in (44).

Comparing (52) with (53), we deduce the following:

(1) Because of the noise enhancement effect arising due to the large time-bandwidth product WT_{R} in (52), for small N_{SAT}, the RAKE can outperform the SAT. But remember, here we assumed that RAKE finger delays (which are not needed by the SAT) are error-free.

(2) When N_{SAT} is large enough, the SAT will outperform the RAKE, which is destined to be an approximation of the ideal matched filter since $L_r \ll L$. In contrast, because SAT can operate blindly, averaging over a sufficient number of symbols will bring SAT performance close to the ideal one without sacrificing rate or interrupting information transmission. In fact, as will be seen in our simulations, it is enough to set $N_{\mathrm{SAT}} > 100$.

(3) As shown in (52), what really determines SAT performance is the product $N_{\mathrm{SAT}}\theta^2$, which suggests an alternative means of approaching the optimal limit, by simply increasing θ. By tuning this parameter, we can mitigate delays in acquisition by keeping N_{SAT} to a small value.

In Section 7, we will validate these observations via simulations performed with pragmatic UWB system parameters.

Remark. In the preceding comparison, we have supplied RAKE with ideal conditions not required by the SAT receiver. First, we have assumed in (45) that RAKE knows $p_{\mathrm{T}}(t)$ perfectly, which is hardly the case due to un-modeled pulse distortions. Furthermore, the TH sequence $\{c_k\}$ embodied in $p_{\mathrm{T}}(t)$ may not be known a priori which will challenge RAKE but not SAT operation. Finally, it is well known that in UWB communications, performance of the RAKE receiver degrades severely even with mistiming in the order of T_p (nanosecond magnitude). However, our SAT receiver will not have this problem. What is more, our SAT recovery module entails timing acquisition, which is not the case for the RAKE receiver. Given all these ideal conditions we have supplied RAKE with, it is truly surprising that SAT can still outperform RAKE for N sufficiently large!

7. Simulations

In this section, we simulate the implementation of our SAT-based algorithms to validate the results developed in this paper. Throughout, BPAM based UWB transmissions are tested using the so called Gaussian (monocycle) pulse shaper $p(t) = 2\sqrt{e}A(t/\tau_g)\exp(-2t^2/\tau_g^2)$, with $\tau_g = 0.2$ ns. At the receiver, the front-end low pass filter has cutoff frequency $W = 4$ GHz, which exceeds the transmission bandwidth (3 dB bandwidth ≈ 3.5 GHz). In (2), we select $T_{\mathrm{f}} = 30$ ns, $N_{\mathrm{f}} = 2$, and $c_0 = c_1 = 0$.

7.1. Performance of SAT

To evaluate the timing and demodulation performance of SAT, we used the multipath channel model "CM 1" from the IEEE 802.15.3a working group [19], having mean excess delay 4.9 ns and RMS delay spread 5 ns. We have verified experimentally that the delay spread of CM1 is effectively upper bounded by 29 ns. After truncation to 29 ns, the channel is normalized to have unit power gain. The A-PAM parameter θ is chosen to be 1 throughout.

(1) *Timing performance*. At 10 and 15 dB receive bit-energy-to-noise ratio, and variable sample size N, the normalized (with respect to T_s^2) mean square errors of the timing estimator $\hat{\tau}_0$ in (13) are plotted in Fig. 3. However, $\hat{\tau}_0$ in (13) and (21) requires searching for the maximum of $J(\tau)$ over a continuous range, which is impossible in practice. Instead, we maximize $J(\tau)$ in (22) over a grid of finite values $\tau = kT_\Delta$, where $k = 0, 1, \ldots, \lfloor 2T_s/T_\Delta \rfloor$, and T_Δ is the sampling period. Let $k^* = \arg\max J(kT_\Delta)$, and define the probability of detection as the probability that k^* equals $k_{\mathrm{opt}} := \arg\min_k |kT_\Delta - \tau_0|$. For 10 dB receive bit-energy-to-noise ratio, this probability for different sampling periods T_Δ is plotted in Fig. 4,

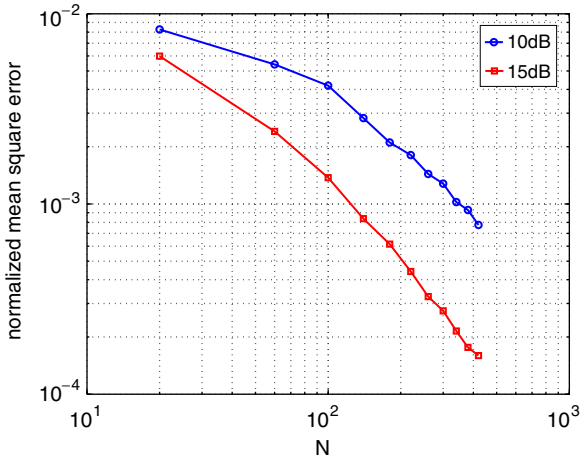

Fig. 3. Normalized mean square error of timing estimator in (13).

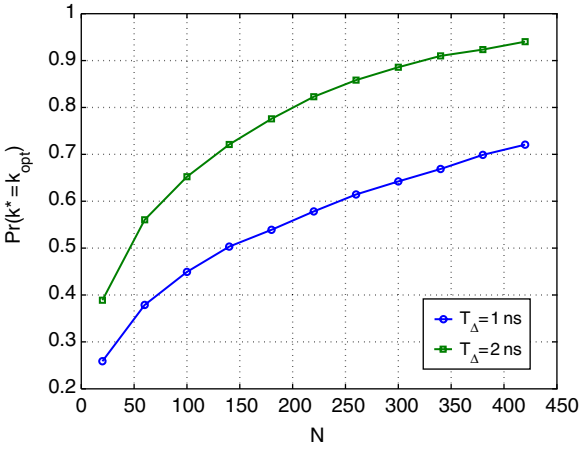

Fig. 4. Probability of detection defined in Section 7.1.

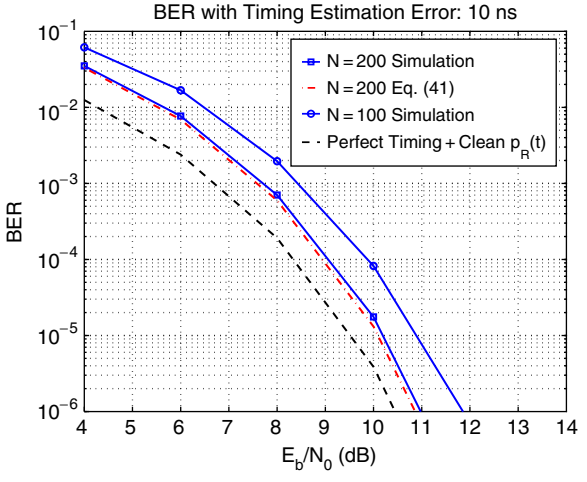

Fig. 5. Detection performance of the SAT-based demodulator.

where we can clearly see that it approaches 1 as N becomes large.

(2) *Detection performance*. In order to test robustness of the SAT receiver to timing errors, we simulate the BER of the detector in (35) with mistiming $\tau_0 - \hat{\tau}_0 = 10\,\text{ns}$, which is more than 10 times T_p. For different sample sizes N, the simulation results are depicted in Fig. 5. In order to check how well (41) approximates the true BER, at fixed

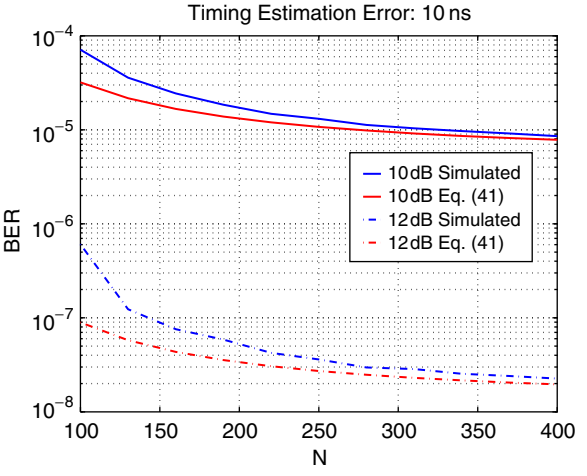

Fig. 6. BER vs. N dependence of the SAT-based demodulator verifying the accuracy of Eq. (41).

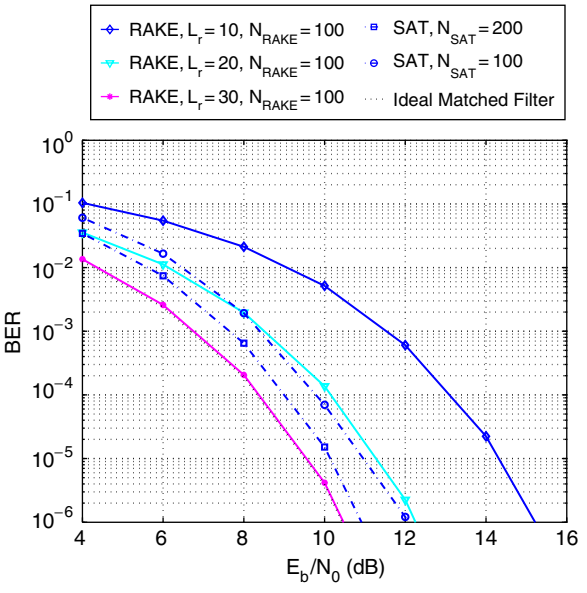

Fig. 7. RAKE vs. SAT comparison at fixed averaging sizes involved in recovering them.

bit-energy-to-noise ratio, we plot the result of (41) along with the simulated BER in Fig. 6. Clearly, the larger N is, the better is the approximation.

7.2. SAT vs. RAKE

In order to capture the dense multipath nature of UWB channels, we adopt the following normalized channel in our subsequent simulations:

$$\tau_{l,0} = l\,\text{ns}, \quad \alpha_l = \pm 1/\sqrt{30}, \quad l = 0, 1, \ldots, 29.$$

Varying the number of RAKE fingers L_r, when $N_{\text{RAKE}} = 100$, the BER of the RAKE receiver is plotted in Fig. 7, where we also depict the BER of the SAT receiver ($\theta = 1$) with $N_{\text{SAT}} = 100$ and 200.

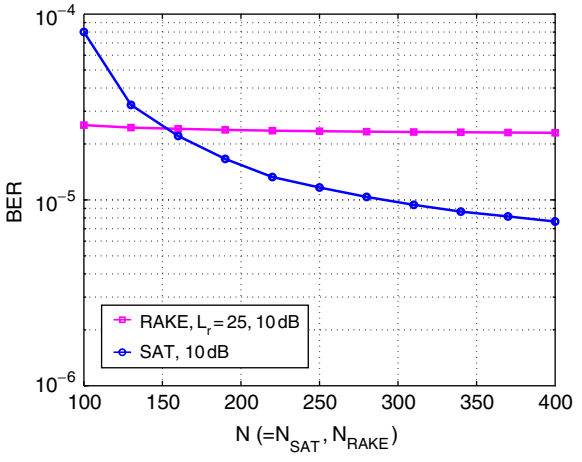

Fig. 8. RAKE vs. SAT comparison at fixed 10 dB bit-energy-to-noise-ratio.

In Fig. 7, we observe that when L_r is small, the SAT receiver performs better than the RAKE. In Fig. 8, we have plotted the BER dependence on the sample size N (N_{SAT} and N_{RAKE}) for a fixed 10 dB bit-energy-to-noise ratio. It is clear that the RAKE receiver's performance is limited by its energy capture, which is determined by L_r. As long as $L_r < L + 1$, i.e., the number of fingers is less than the total number of multipath returns, the SAT will outperform the RAKE beyond a certain finite averaging size N_{SAT} which can be as small as 100 in practical settings.

8. Concluding summary

In this paper, we have generalized and analyzed low-complexity timing and demodulation modules based on the synchronized aggregate template (SAT) recovered using a judiciously designed periodically nonzero mean transmission pattern that can rely on either BPAM or BPPM. The proposed algorithms are applicable even in the harshest scenario, where ISI and MUI are simultaneously present. Unlike the widely adopted RAKE receiver, the SAT demodulator can be very robust to timing estimation error. Even with perfect timing information, RAKE reception in the UWB regime suffers from limited energy that can be captured with an affordable number of fingers. On the other hand, our SAT demodulator can achieve full multipath diversity at low-complexity. As a concluding remark, we have listed the characteristics of SAT in comparison with RAKE in Table 1, from which one can appreciate the great potential SAT based algorithms have for deployment.

Table 1
Comparative characteristics of SAT and RAKE

SAT	RAKE
Low complexity: • No need for individual path estimation • Single correlator (RF chain) needed • Simple tracking algorithm [7]	High complexity: • Need to estimate many individual paths for combining • Large number of correlators needed • Resource consuming tracking: all fingers need for real-time updating
Effective energy capture: • Full multipath diversity	Ineffective energy capture: • Limited diversity
Robustness to: • Timing errors • Un-modeled pulse distortion	Sensitively to: • Timing errors • Un-modeled pulse distortion

References

[1] L. Yang, G.B. Giannakis, Ultra-wideband communications: an idea whose time has come, IEEE Signal Process. Mag. 21 (6) (November 2004) 26–54.

[2] E.A. Homier, R.A. Scholtz, Rapid acquisition of ultra-wideband signals in the dense multi-path channels, in: Proceedings of Conference on Ultra-Wideband Systems and Technologies, Baltimore, MD, May 20–23, 2002, pp. 105–110.

[3] Z. Tian, G.B. Giannakis, A GLRT approach to data-aided timing acquisition in UWB radios—parts I/II, IEEE Trans. Wireless Comm. 4 (6) (2005) 2956–2967/2994–3004.

[4] V. Lottici, A.D. Andrea, U. Mengali, Channel estimation for ultra-wideband communications, IEEE J. Select. Areas Comm. 20 (December 2002) 1638–1645.

[5] L. Yang, G.B. Giannakis, Blind UWB timing with a dirty template, in: Proceedings of International Conference on ASSP, Montreal, Quebec, Canada, May 2004; See also Proceedings of GLOBECOM Conference, San Francisco, CA, December 2003, pp. 769–773.

[6] Z. Wang, X. Yang, Blind channel estimation for ultra wideband communications employing pulse position modulation, IEEE Signal Process. Lett. 12 (7) (July 2005) 520–523.

[7] X. Luo, G.B. Giannakis, Low-complexity blind synchronization and demodulation for (ultra-) wideband multi-user ad hoc access, IEEE Trans. Wireless Comm. (2006), to appear. Available at: ⟨http://spincom.ece.umn.edu/papers04/twc06xluo.pdf⟩.

[8] M.Z. Win, R.A. Scholtz, On the energy capture of ultrawide bandwidth signals in dense multipath environments, IEEE Comm. Lett. 2 (9) (September 1998) 245–247.

[9] H. Niu, J.A. Ritcey, H. Liu, Performance of UWB RAKE receivers with imperfect tap weights, in: Proceedings of International Conference on ASSP, vol. 4, Hong Kong, China, April 4–6, 2003, pp. 125–128.

[10] H. Sheng, R. You, A.M. Haimovich, Performance analysis of ultra-wideband RAKE receivers with channel delay estimation errors, in: Proceedings of the 38th Conference on Information Sciences and Systems, Princeton, New Jersey, March 17–19, 2004, pp. 921–926.

[11] Z. Tian, G.B. Giannakis, BER sensitivity to mis-timing in ultra-wideband communications, part I: non-random channels, IEEE Trans. Signal Process. 53 (4) (April 2005) 1550–1560.

[12] R. Hoctor, H. Tomlinson, Delay-hopped transmitted-reference RF communications, in: Proceedings of IEEE Conference on UWB Systems and Technologies, Baltimore, MD, May 2002, pp. 265–269.

[13] L. Yang, G.B. Giannakis, Optimal pilot waveform assisted modulation for ultrawideband communications, IEEE Trans. Wireless Comm. 3 (4) (July 2004) 1236–1249.

[14] M.-H. Chung, R.A. Scholtz, Comparison of transmitted- and stored-reference systems for ultra-wideband communications, in: Proceedings of MILCOM Conference, Monterey, CA, October 31–November 3, 2004.

[15] L. Wu, X. Wu, Z. Tian, RAKE versus noisy template based UWB receivers under timing and channel estimation errors, in: Proceedings of the International Conference on Communications, Seoul, Korea, May 16–20, 2005.

[16] IEEE P802.15 working group for WPANs, Time variance for UWB wireless channels, IEEE P802.15-02/461r1-SG3a, November 2002.

[17] L. Miller, J. Lee, Error analysis of time delay estimation using a finite integration time correlator, IEEE Trans. Signal Process. 29 (3) (June 1981) 490–496.

[18] J.G. Proakis, Digital Communications, fourth ed., McGraw-Hill, New York, 2001 (Chapter 5).

[19] IEEE P802.15 working group for WPANs, Channel modeling sub-committee report final, IEEE P802.15-02/368r5-SG3a, November 2002.